ACS APPLIED MATERIALS & INTERFACES

Letter

Photoresponsive Bridged Silsesquioxane Nanoparticles with Tunable Morphology for Light-Triggered Plasmid DNA Delivery

Yevhen Fatieiev, Jonas Croissant, Shahad Alsaiari, Basem A Moosa, Dalaver H. Anjum, and Niveen M Khashab

ACS Appl. Mater. Interfaces, **Just Accepted Manuscript** • DOI: 10.1021/acsami.5b07365 • Publication Date (Web): 25 Sep 2015

Just Accepted

ACS Publications

ACS Applied Materials & Interfaces is published by the American Chemical Society.
1155 Sixteenth Street N.W., Washington, DC 20036

Photoresponsive Bridged Silsesquioxane Nanoparticles with Tunable Morphology for Light-Triggered Plasmid DNA Delivery

Yevhen Fatieiev,‡ Jonas G. Croissant,‡ Shahad Alsaiari, Basem A. Moosa, Dalaver H. Anjum, and Niveen M. Khashab*

Smart Hybrid Materials Laboratory (SHMs), Imaging and Characterization Laboratory, Advanced Membranes and Porous Materials Center, King Abdullah University of Science and Technology (KAUST), Thuwal 23955-6900, Kingdom of Saudi Arabia.

ABSTRACT: Bridged silsesquioxane nanocomposites with tunable morphologies incorporating *o*-nitrophenylene-ammonium bridges are described. The systematic screening of the sol-gel parameters allowed the material to reach the nanoscale with controlled dense and hollow structures of 100 to 200 nm. The hybrid composition of silsesquioxanes with 50% of organic content homogenously distributed in the nanomaterials endowed them with photoresponsive properties. Light irradiation was performed to reverse the surface charge of nanoparticles from +46 to -39 mV via the photoreaction of the organic fragments within the particles, as confirmed by spectroscopic monitorings. Furthermore, such nanoparticles were applied for the first time for the on-demand delivery of plasmid DNA in HeLa cancer cells via light actuation.

KEYWORDS: *bridged silsesquioxane, DNA delivery, organosilica, hollow nanoparticles, charge reversal*

Bridged silsesquioxane (BS) nanomaterials with chemical structures $O_{1.5}Si\text{-}R\text{-}SiO_{1.5}$ with organic R groups are emerging as the next generation of organosilica nanocomposites.[1-9] Nonetheless, it remains a challenge to control the kinetic in sol-gel processes, which generally lead to macroscaled nonporous BS functional materials.[10-12] Their design involves kinetically-controlled sol-gel processes of bis- or multi-organoalkoxysilanes which yield to hybrid materials with very high organic contents depending on the type of organic groups.[1] BS materials substantially differ with organically-modified silica, also called ORMOSIL, which are organically-doped silica materials and thus possess lower organic contents. Consequently, the BS matrix photophysical, chemical, thermal and mechanical properties are governed by the homogenously distributed organic fragments within the siloxane network.[13] Thus, BS materials with features such as luminescence,[14] magnetism,[15] and self-assembly were designed[16] for various applications including catalysis,[17] solid-state lightning,[18] energy and electronics.[13]

Nanoscaled BS materials are thus highly desirable in this day of miniaturized devices and nanocomposite materials. Shea *et al.* pioneered BS nanoparticles (NPs) with photodeformable particles based on coumarin dimer bridges.[3] The material was composed of 100 nm aggregated spherical particles. The same group later reported bipyridinium- and ethylenediamine-based BS spherical monodisperse particles,[4] as well as phenylene, alkylene, and aminoalkyl bridges.[19] Recently, few studies described BS NPs for biomedical applications, namely drug delivery with cis-platin bridges as prodrug,[20] MRI imaging[21] with BS NPs composed of gadolinium-complexed bridges. Croissant *et al.* reported BS and gold core BS shell NPs designed from a tetra-alkoxysilylated two-photon photosensitizer and efficiently applied them for two-photon fluorescence imaging and photodynamic therapy in cancer cells.[1] They recently designed disulfide-based biodegradable BS NPs chemically-doped with diphenylbutadiene and porphyrin photosensitizers for two-photon photodynamic therapy and imaging in-vitro.[22] BS NPs with charge reversal from negative to positive values were reported with aminopropyl-bridges with *o*-nitrobenzyl pending groups and applied for light-triggered hydrogel assembly and plastic antibody release.[23] Reported BS nanomaterials were almost exclusively dense nanospheres, with the exception of perylenediimide-bridged nanoribbons endowed with electronic properties obtained by Hammer and co-workers, and several microfibers with diameters of few hundred nanometres.[24] The aggregation of BS NPs is often observed and remains a major drawback for future biomedical applications. Ideally, BS NPs should be non-aggregated sub-200 nm nanomaterials to benefit the enhanced permeation and retention (EPR) effect and thus accumulate in cancerous tissues and organs. The delivery of plasmid DNA was achieved with ORMOSIL and mesoporous silica NPs,[25-26] but not with BS NPs, and necessitated complex multi-step postfunctionalizations of polymer and coupling agent.

Herein we report the controlled syntheses of sub-200 nm non-aggregated BS nanospheres with tunable morphology with dense or hollow nanostructure designed from sol-gel processes of a photoresponsive bridged alkoxysilane (PBA) precursor (see Figure 1). The unique constitution of these BS NPs enables the on-demand surface charge reversal via light-trigger from positive to negative charges. Furthermore, this feature was harnessed to apply BS nanocarriers without further functionalization for the first time for light-triggered plasmid DNA delivery in cancer cells.

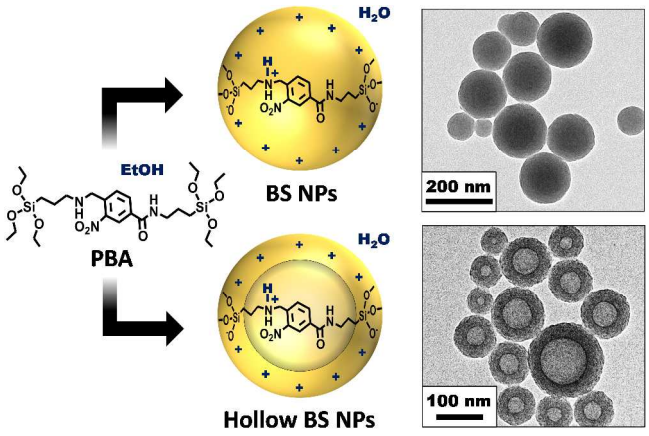

Figure 1. Design of BS and hollow BS NPs via the sol-gel reactions of the PBA precursor, as shown by TEM micrographs.

The PBA precursor, of IUPAC name 3-nitro-N-(3-(triethoxysilyl)propyl)-4-(((3-(triethoxysilyl)propyl)amino)-methyl)benzamide, was first synthesized and characterized. The synthesis involved a soft chlorination of 4-(bromomethyl)-3-nitrobenzoic acid followed by a coupling with 2 equivalent of 3-aminopropyltriethoxysilane in dichloromethane under base-catalysis at 0°C (ESI, Figure S1).[27] The chemical structure of the precursor was confirmed via proton and carbon nuclear magnetic resonance (NMR) and Fourier transform infrared (FTIR) spectroscopies (Figures S2 and S3).

BS nanomaterials were then synthesized via sol-gel methods. Controlled designs of BS NPs with different morphologies were achieved via a modified Stöber method.[28] An aqueous mixture containing cetyltrimethylammonium bromide (CTAB), sodium hydroxide catalyst, and an ethanol co-solvent was prepared at 75°C. Then, the hydrolysis-condensation of the PBA precursor was conducted for 2 h. Such conditions lead to the formation of BS NPs with size under 200 nm, as shown by transmission electron microscopy (TEM) image (see top image in Figure 1). Interestingly, we unexpectedly found that without the use of CTAB in a certain range of temperature, pH, and alkoxysilane concentration the formation of the hollow BS nanostructure was observed (see bottom image in Figure 1). In fact, the diameter of NPs as well the formation of the hollow or non-hollow structure could be tuned by varying four parameters: pH, temperature, alkoxysilane concentration and type of alcohol co-solvent (see Figure S4, Tables S1 and S2). The formation of hollow particles could be achieved from 50 to 90°C and pH 11 to 12 (Figures S4B-C), while no correlation was observed between the size and temperature. The possibility to form hollow BS NPs with methanol, ethanol, and i-propanol co-solvent (and not from butanol) suggests the formation of nanoemulsions in specific conditions which promote hollow particle nanostructuration (Figure S4D).

The size, morphology, and composition of BS nanomaterials were further investigated via various techniques. Scanning electron microscopy (SEM) micrographs displayed relatively monodisperse BS and hollow BS spherical NPs (See Figures S5A-B), with dynamic light-scattering (DLS) average hydrodynamic diameters of 190 and 106 nm respectively (Figure S5C-D), which is in accordance with microscopy images and the hydration layer on NPs. The incorporation of organic bridges into the silica framework of BS and hollow BS NPs was proved by Fourier transform infrared (FTIR) spectroscopy with the $\nu_{C=O}$ at 1645 cm^{-1}, ν_{N-H} at 3289 cm^{-1}, ν_{N-O} at 1535 cm^{-1}, as well as aliphatic and aromatic C-H stretching modes (see Figure S6). The high degree of condensation of siloxanes was confirmed by the shift of the ν_{Si-O} value from 1090 to 1130 cm^{-1}. Thermogravimetric analysis (TGA) of BS and hollow BS NPs also confirmed the high organic content of the nanocomposites with two significant weight losses at 220 and 480°C according to the first derivative of the thermogravimetric (DTG) curve, leading to a total weight loss of 48% (Figures S7 and S8). Moreover, we utilized spectrum imaging (SI) in scanning transmission electron microscopy (STEM) combined with electron energy-loss spectroscopy (EELS) to assess the homogeneity in composition of hollow BS NPs. Spectra were acquired (see one in Figure S9) at each pixel image (~1 nm) on a representative particle, and the elemental mappings of silicon, oxygen, nitrogen and carbon were extracted (Figure 2). The results clearly exhibit the homogenous dispersion of the organic moieties within the NPs framework. This conclusion was further supported by the homogeneous composition of these elements along the diameter of hollow BS NPs (see Figure S10). Additionally, we also successfully prepared rhodamine B-doped hollow BS NPs of 50 nm with homogenous composition of dye in the nanostructure (Figure S11).

The light-responsiveness of the BS nanomaterials was then assessed and monitored spectroscopically. In a typical experiment,

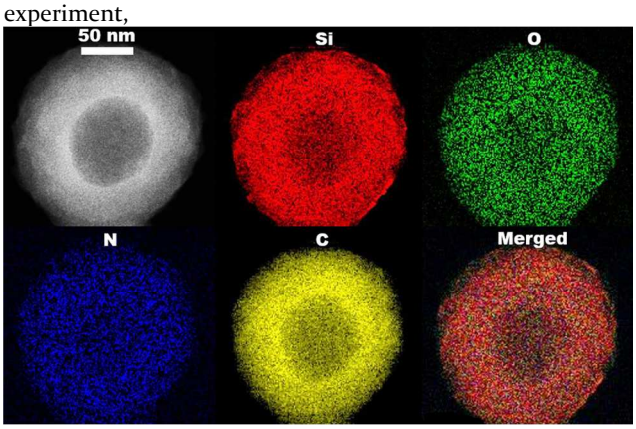

Figure 2. STEM-EELS elemental mapping (silicon, oxygen, nitrogen, carbon) of a representative hollow BS NP. The merged image consists of silicon, nitrogen, and oxygen.

an aqueous suspension of NPs was irradiated with UV-light at 365 nm (24.6 $mW.cm^{-2}$). We first analysed the irradiation of the positively-charged *o*-nitrophenylene-ammonium PBA precursor which caused a classic internal photocleavage[29-30] leading to the formation of the neutral the nitrosophenyleneimine derivative (Figure 3A), as shown by the disappearance of the benzyl protons in the NMR spectrum (see Figure S12). This was supported by the appearance of the shift of the 285 nm phenyl band in the UV-Visible spectrum (Figure S13), and the shift of the symmetric stretching ν_{N-O} vibration mode from 1540 to 1550 cm^{-1} (Figure S14). However, the same trends were observed in BS nanomaterials (Figure 3B-C, see FTIR ν_{N-O} shift in Figure S15). The photo- reaction monitored via UV-Visible spectroscopy was found to necessitate 10 minutes of irradiation for a full conversion (see Figure 3C), which was accompanied by a progressive modification of the surface charge of BS NPs from +46 to -5, -30 and -39 mV after 4, 8,

and 10 minutes of irradiation respectively (see Figure 4A, and Figure S16). Upon illumination, *o*-nitrophenylene-

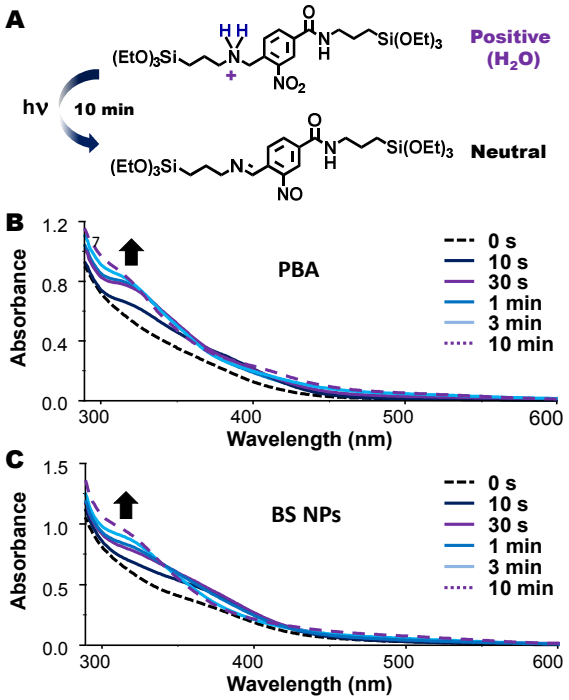

Figure 3. Photoreaction of the PBA precursor (A). UV-Visible spectroscopy monitoring of the photoreaction in the PBA in absolute ethanol (B) and in BS NPs in water (C) before and after irradiation for different time intervals.

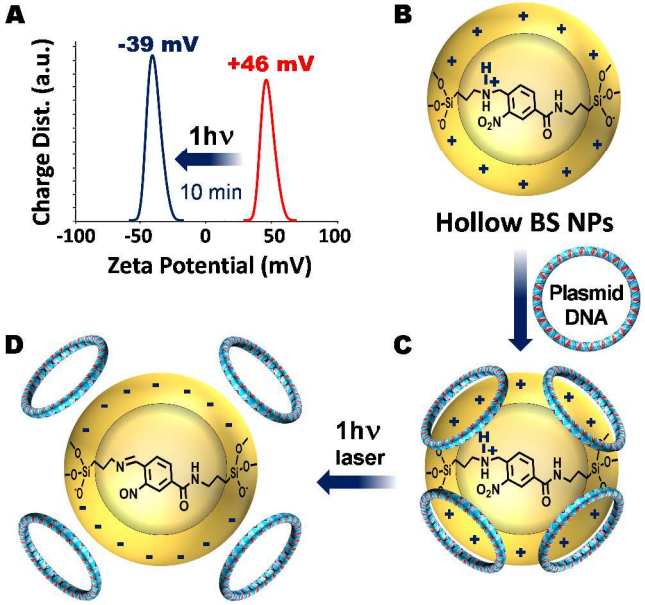

Figure 4. Zeta potential measurements on BS NPs before and after irradiation, depicting the NPs surface charge reversal (A). Schematic representation of positively-charged BS NPs (B) which electrostatically bind DNA strands (C) for light-triggered delivery (D). The negative charge of NPs results from the neutralisation of the charge of the organic bridges.

ammonium moieties on the surface of BS NPs turned into neutral nitrosophenylene-imine moieties, which resulted in a negative surface charge afforded by silanolates groups (see Figure S17).

The unique charge reversal feature was thus applied for the electrostatic binding of negatively charged plasmid DNA and its subsequent delivery to a cancer cell line in culture (Figure 4B-D). BS NPs were found to be tolerated by in HeLa cells, as shown by less than 10% of cytotoxicity up to 20 $\mu g.mL^{-1}$ (Figure S18). The electrostatic binding of DNA (60 pb, ~20 nm) on positively charged BS NPs was confirmed via gel electrophoresis and zeta potential measurements, with 7.5 ng of bound DNA per microgram of NPs (Figures S19 and S20). HeLa cancer cells were then incubated with BS-DNA NPs at 11 $\mu g.mL^{-1}$ for 12 hours. Nuclei were stained with 4',6-diamidino-2-phenylindole (DAPI), and the delivery of plasmid DNAs was assessed via the production of the green fluorescent protein (GFP) as reporter gene. Indeed, the fluorescence of GFP necessitates the transcription of DNA in the nucleus with subsequent mRNA translation, which implies the detachment of DNA from BS NPs given the small pore sizes of nuclei (≤10 nm).[26] Confocal laser scanning microscopy (CLSM) images were thus acquired to determine the DNA delivery capability of the designed hollow BS NPs (see Figure 5). Before irradiation, a small amount of GFP could be seen, which indicated that few DNA were autonomously delivered to cells via NPs (Figure 5A). However, when the irradiation was turned on (365 nm, 25 mW, 4x10 s), a sufficient amount of DNA was delivered in the cytosol (see Figure 5B) through photo-induced electrostatic repulsions (Figures 4C-D). This effect was also clearly seen after only 6 h of incubation (Figure S21). Notably, zeta potential measurements for BS NPs didn't show full charge reversal from positive to negative after 40 s of UV-irradiation. Although, it was enough to decrease electrostatic binding and consequently increase repulsions between negatively charge silanolates groups and DNA. As a result, partial release of DNA from the surface of BS-DNA NPs was observed (Figure S20). Note that, single stranded DNA were also attached to BS NPs (53 $ng.mg^{-1}$) and transported and tracked via Cy3 cyanine labelling, while bright field images showed the intracellular co-localizations of aggregated BS NPs and DNA-Cy3 fluorescence (Figure S22).

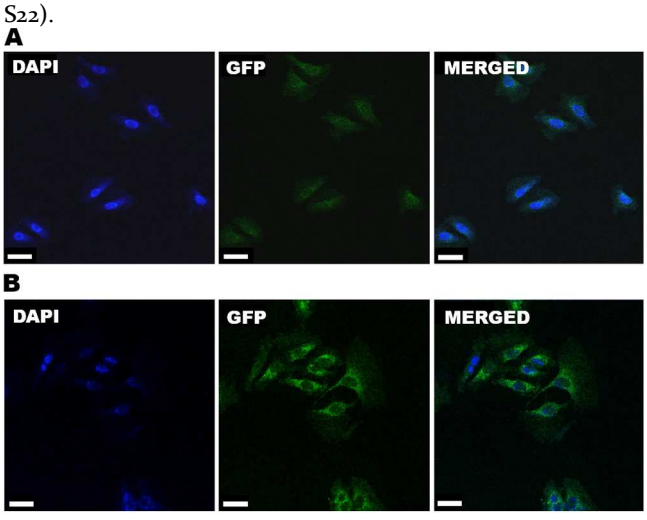

Figure 5. CLSM images on HeLa cells after 12 h of incubation with non-irradiated (A) and irradiated BS NPs binding DNA strands (B). Nuclei are stained in blue with DAPI. DNA is tracked via GFP fluorescing in green, thus proving the DNA delivery from BS NPs. Scale bars of 40 µm.

In summary, we report the syntheses of bridged silsesquioxane nanomaterials with tunable size and morphology, affording non-aggregated dense or hollow nanospheres. The organic-inorganic nanomaterials possessed a very high organic content (~50%) of photoresponsive fragments which enabled the on-demand charge reversal from positive to negative values. The hybrid compositions of the designed materials were investigated via various techniques and found to be homogenous in the NPs, while its photoresponsiveness was monitored spectroscopically. By way of proof of principle of the biomedical application of these BS NPs, light-triggered delivery of plasmid DNA to cancer cells in culture was demonstrated for the first time. The light-actuation was found to be effectively delivering DNA while the non-irradiated nanomaterials did not induce significant gene expressions. Dye-doped hollow BS NPs are envisioned for biomedical imaging while the use of a near-infrared fluorophore could extend its potential for in-vivo biomedical applications.

■ ASSOCIATED CONTENT

Supporting Information

Supplementary experimental sections, additional characterization data of the PBA, BS and hollow BS NPs, and data of *in vitro* studies. This material is available free of charge via the Internet at http://pubs.acs.org.

■ AUTHOR INFORMATION

Corresponding Author

E-mail: Niveen.khashab@kaust.edu.sa Tel: +966-28021172. Fax: +966-28082410.

Author Contributions

‡These authors contributed equally. All authors contributed to the work.

Notes

The authors declare no competing financial interests.

■ ACKNOWLEDGMENTS

We gratefully acknowledge support from King Abdullah University of Science and Technology (KAUST).

■ REFERENCES

(1) Croissant, J.; Maynadier, M.; Mongin, O.; Hugues, V.; Blanchard-Desce, M.; Chaix, A.; Cattoën, X.; Wong Chi Man, M.; Gallud, A.; Gary-Bobo, M.; Garcia, M.; Raehm, L.; Durand, J.-O. Enhanced Two-Photon Fluorescence Imaging and Therapy of Cancer Cells via Gold@Bridged Silsesquioxane Nanoparticles. *Small* **2015**, *11*, 295–299.

(2) Xu, L.; Manda, V. R.; McNamara, L. E.; Jahan, M. P.; Rathnayake, H.; Hammer, N. I. Covalent Synthesis of Perylenediimide-Bridged Silsesquioxane Nanoribbons and Their Electronic Properties. *RSC Adv.* **2014**, *4*, 30172–30179.

(3) Zhao, L.; Loy, D. A.; Shea, K. J. Photodeformable Spherical Hybrid Nanoparticles. *J. Am. Chem. Soc.* **2006**, *128*, 14250–14251.

(4) Khiterer, M.; Shea, K. J. Spherical, Monodisperse, Functional Bridged Polysilsesquioxane Nanoparticles. *Nano Lett.* **2007**, *7*, 2684–2687.

(5) Croissant, J.; Salles, D.; Maynadier, M.; Mongin, O.; Hugues, V.; Blanchard-Desce, M.; Cattoën, X.; Wong Chi Man, M.; Gallud, A.; Garcia, M.; Gary-Bobo, M.; Raehm, L.; Durand, J.-O. Mixed Periodic Mesoporous Organosilica Nanoparticles and Core–Shell Systems, Application to in Vitro Two-Photon Imaging, Therapy, and Drug Delivery. *Chem. Mater.* **2014**, *26*, 7214–7220.

(6) Croissant, J.; Cattoën, X.; Wong Chi Man, M.; Dieudonné, P.; Charnay, C.; Raehm, L.; Durand, J.-O. One-Pot Construction of Multipodal Hybrid Periodic Mesoporous Organosilica Nanoparticles with Crystal-Like Architectures. *Adv. Mater.* **2015**, *27*, 145–149.

(7) Fatieiev, Y.; Croissant, J. G.; Julfakyan, K.; Deng, L.; Anjum, D. H.; Khashab, N. M. Enzymatically Degradable Hybrid Organic-Inorganic Bridged Silsesquioxane Nanoparticles for In-Vitro Imaging. **2015**, *7*, 15046–15050.

(8) Blanco, I.; Abate, L.; Bottino, F. A.; Cicala, G.; Latteri, A. Dumbbell-Shaped Polyhedral Oligomeric Silsesquioxanes/ Polystyrene Nanocomposites: The Influence of the Bridge Rigidity on the Resistance to Thermal Degradation. *J. Compos. Mater.* **2015**, *49*, 2509–2517.

(9) Blanco, I.; Abate, L.; Bottino, F. Synthesis and Thermal Characterization of New Dumbbell-Shaped Cyclopentyl-Substituted POSSs Linked by Aliphatic and Aromatic Bridges. *J. Therm. Anal. Calorim.* **2015**, *121*, 1039–1048.

(10) Loy, D. A.; Shea, K. J. Bridged Polysilsesquioxanes. Highly Porous Hybrid Organic-Inorganic Materials. *Chem. Rev.* **1995**, *95*, 1431–1442.

(11) Shea, K. J.; Loy, D. A. Bridged polysilsesquioxanes. Molecular-Engineered Hybrid Organic-Inorganic Materials. *Chem. Mater.* **2001**, *13*, 3306–3319.

(12) Moreau, J. J.; Pichon, B. P.; Wong Chi Man, M.; Bied, C.; Pritzkow, H.; Bantignies, J. L.; Dieudonné, P.; Sauvajol, J. L. A Better Understanding of the Self-Structuration of Bridged Silsesquioxanes. *Angew. Chem., Int. Ed.* **2004**, *43*, 203–206.

(13) Hu, L.-C.; Shea, K. J. Organo-Silica Hybrid Functional Nanomaterials: How Do Organic Bridging Groups and Silsesquioxane Moieties Work Hand-In-Hand? *Chem. Soc. Rev.* **2011**, *40*, 688–695.

(14) Nobre, S. S.; Cattoën, X.; Ferreira, R. A.; Carcel, C.; de Zea Bermudez, V.; Wong Chi Man, M.; Carlos, L. D. Eu^{3+}-Assisted Short-Range Ordering of Photoluminescent Bridged Silsesquioxanes. *Chem. Mater.* **2010**, *22*, 3599–3609.

(15) Wu, L.; Chen, Q.; Lv, Z.; Sun, W.; Chen, L.; Wu, J. Bithiazole-Bridged Polysilsesquioxane and Its Metal Complexes: Synthesis and Magnetic Properties. *J. Sol-Gel Sci. Technol.* **2011**, *60*, 214–220.

(16) Creff, G.; Pichon, B. P.; Blanc, C.; Maurin, D.; Sauvajol, J.-L.; Carcel, C.; Moreau, J. J. E.; Roy, P.; Bartlett, J. R.; Wong Chi Man, M.; Bantignies, J.-L. Self-Assembly of Bridged Silsesquioxanes: Modulating Structural Evolution via Cooperative Covalent and Noncovalent Interactions. *Langmuir* **2013**, *29*, 5581–5588.

(17) Monge-Marcet, A.; Pleixats, R.; Cattoën, X.; Man, M. W. C.; Alonso, D. A.; Nájera, C. Prolinamide Bridged Silsesquioxane as an Efficient, Eco-Compatible and Recyclable Chiral Organocatalyst. *New J. Chem.* **2011**, *35*, 2766–2772.

(18) Graffion, J.; Cattoën, X.; Freitas, V. T.; Ferreira, R. A.; Man, M. W. C.; Carlos, L. D. Engineering of Metal-Free Bipyridine-Based Bridged Silsesquioxanes for Sustainable Solid-State Lighting. *J. Mater. Chem.* **2012**, *22*, 6711–6715.

(19) Hu, L.-C.; Khiterer, M.; Huang, S.-J.; Chan, J. C. C.; Davey, J. R.; Shea, K. J. Uniform, Spherical Bridged Polysilsesquioxane Nano- and Microparticles by a Nonemulsion Method. *Chem. Mater.* **2010**, *22*, 5244–5250.

(20) Rocca, J. D.; Werner, M. E.; Kramer, S. A.; Huxford-Phillips, R. C.; Sukumar, R.; Cummings, N. D.; Vivero-Escoto, J. L.; Wang, A. Z.; Lin, W. Polysilsesquioxane Nanoparticles for Triggered Release of Cisplatin and Effective Cancer

Chemoradiotherapy. *Nanomedicine (N. Y., NY, U. S.)* **2015**, *11*, 31–38.

(21) Vivero-Escoto, J. L.; Rieter, W. J.; Lau, H.; Huxford-Phillips, R. C.; Lin, W. Biodegradable Polysilsesquioxane Nanoparticles as Efficient Contrast Agents for Magnetic Resonance Imaging. *Small* **2013**, *9*, 3523–3531.

(22) Croissant, J. G.; Mauriello-Jimenez, C.; Cattoën, X.; Wong Chi Man, M.; Raehm, L.; Maynadier, M.; Gary-Bobo, M.; Garcia, M.; Maillard, P.; Durand, J.-O. Synthesis of Disulfide-Based Biodegradable Bridged Silsesquioxane Nanoparticles for Two-Photon Imaging and Therapy of Cancer Cells. *Chem. Commun.* **2015**, *51*, 12324–12327.

(23) Hu, L.-C.; Yonamine, Y.; Lee, S.-H.; van der Veer, W. E.; Shea, K. J. Light-Triggered Charge Reversal of Organic–Silica Hybrid Nanoparticles. *J. Am. Chem. Soc.* **2012**, *134*, 11072–11075.

(24) Llusar, M.; Sanchez, C. Inorganic and Hybrid Nanofibrous Materials Templated with Organogelators. *Chem. Mater.* **2008**, *20*, 782–820.

(25) Roy, I.; Ohulchanskyy, T. Y.; Bharali, D. J.; Pudavar, H. E.; Mistretta, R. A.; Kaur, N.; Prasad, P. N. Optical Tracking Of Organically Modified Silica Nanoparticles as DNA Carriers: a Nonviral, Nanomedicine Approach for Gene Delivery. *Proc. Natl. Acad. Sci. U. S. A.* **2005**, *102*, 279–284.

(26) Torney, F.; Trewyn, B. G.; Lin, V. S. Y.; Wang, K. Mesoporous Silica Nanoparticles Deliver DNA and Chemicals into Plants. *Nat. Nanotechnol.* **2007**, *2*, 295–300.

(27) Li, S.; Moosa, B. A.; Croissant, J. G.; Khashab, N. M. Electrostatic Assembly/Disassembly of Nanoscaled Colloidosomes for Light-Triggered Cargo Release. *Angew. Chem., Int. Ed.* **2015**, *127*, 6908–6912.

(28) Kresge, C. T.; Leonowicz, M. E.; Roth, W. J.; Vartuli, J. C.; Beck, J. S. Ordered Mesoporous Molecular Sieves Synthesized By Liquid-Crystal Template Mechanism. *Nature* **1992**, *359*, 710–712.

(29) Il'ichev, Y. V.; Schwörer, M. A.; Wirz, J. Photochemical Reaction Mechanisms of 2-Nitrobenzyl Compounds: Methyl Ethers and Caged ATP. *J. Am. Chem. Soc.* **2004**, *126*, 4581–4595.

(30) Smet, M.; Liao, L.-X.; Dehaen, W.; McGrath, D. V. Photolabile Dendrimers Using o-Nitrobenzyl Ether Linkages. *Org. Lett.* **2000**, *2*, 511–513.

TOC